

Article

An Accurate Metaheuristic Mountain Gazelle Optimizer for Parameter Estimation of Single- and Double-Diode Photovoltaic Cell Models

Rabeh Abbassi ^{1,2,3,*} , Salem Saidi ^{2,4} , Shabana Urooj ^{5,*} , Bilal Naji Alhasnawi ⁶ , Mohamad A. Alawad ⁷  and Manoharan Premkumar ⁸ 

- ¹ Department of Electrical Engineering, College of Engineering, University of Ha'il, Ha'il City 81451, Saudi Arabia
 - ² LaTICE Laboratory, Higher National Engineering School of Tunis (ENSIT), University of Tunis, 5 Avenue Taha Hussein, P.O. Box 56, Tunis 1008, Tunisia; salem.saidi@enstab.ucar.tn
 - ³ Institute of Applied Sciences and Technology of Kasserine (ISSATKas), University of Kairouan, P.O. Box 471, Kasserine 1200, Tunisia
 - ⁴ National School of Advanced Sciences and Technologies of Borj Cédria (ENSTAB), University of Carthage, P.O. Box 122, Hammam-Chott 1164, Tunisia
 - ⁵ Department of Electrical Engineering, College of Engineering, Princess Nourah bint Abdulrahman University, P.O. Box 84428, Riyadh 11671, Saudi Arabia
 - ⁶ Department of Electricity Techniques, Al-Samawah Technical Institute, Al-Furat Al-Awsat Technical University, Kufa 66001, Iraq; bilalnaji1@yahoo.com
 - ⁷ Department of Electrical Engineering, Imam Mohammad Ibn Saud Islamic University, Riyadh 11564, Saudi Arabia; maawaad@imamu.edu.sa
 - ⁸ Department of Electrical and Electronics Engineering, Dayananda Sagar College of Engineering, Bengaluru 560078, Karnataka, India; drpremkumar-eee@dayanandasagar.edu
- * Correspondence: r.abbassi@uoh.edu.sa (R.A.); smurooj@pnu.edu.sa (S.U.)



Citation: Abbassi, R.; Saidi, S.; Urooj, S.; Alhasnawi, B.N.; Alawad, M.A.; Premkumar, M. An Accurate Metaheuristic Mountain Gazelle Optimizer for Parameter Estimation of Single- and Double-Diode Photovoltaic Cell Models. *Mathematics* **2023**, *11*, 4565. <https://doi.org/10.3390/math11224565>

Academic Editors: Pedro Navas and Bo Li

Received: 9 October 2023

Revised: 1 November 2023

Accepted: 3 November 2023

Published: 7 November 2023



Copyright: © 2023 by the authors. Licensee MDPI, Basel, Switzerland. This article is an open access article distributed under the terms and conditions of the Creative Commons Attribution (CC BY) license (<https://creativecommons.org/licenses/by/4.0/>).

Abstract: Accurate parameter estimation is crucial and challenging for the design and modeling of PV cells/modules. However, the high degree of non-linearity of the typical I–V characteristic further complicates this task. Consequently, significant research interest has been generated in recent years. Currently, this trend has been marked by a noteworthy acceleration, mainly due to the rise of swarm intelligence and the rapid progress of computer technology. This paper proposes a developed Mountain Gazelle Optimizer (MGO) to generate the best values of the unknown parameters of PV generation units. The MGO mimics the social life and hierarchy of mountain gazelles in the wild. The MGO was compared with well-recognized recent algorithms, which were the Grey Wolf Optimizer (GWO), the Squirrel Search Algorithm (SSA), the Differential Evolution (DE) algorithm, the Bat–Artificial Bee Colony Optimizer (BABCO), the Bat Algorithm (BA), Multiswarm Spiral Leader Particle Swarm Optimization (M-SLPSO), the Guaranteed Convergence Particle Swarm Optimization algorithm (GCPSO), Triple-Phase Teaching–Learning–Based Optimization (TPTLBO), the Criss-Cross-based Nelder–Mead simplex Gradient-Based Optimizer (CCNMGBO), the quasi-Opposition-Based Learning Whale Optimization Algorithm (OBLWOA), and the Fractional Chaotic Ensemble Particle Swarm Optimizer (FC-EPHO). The experimental findings and statistical studies proved that the MGO outperformed the competing techniques in identifying the parameters of the Single-Diode Model (SDM) and the Double-Diode Model (DDM) PV models of Photowatt-PWP201 (polycrystalline) and STM6-40/36 (monocrystalline). The RMSEs of the MGO on the SDM and the DDM of Photowatt-PWP201 and STM6-40/36 were 2.042717×10^{-3} , 1.387641×10^{-3} , 1.719946×10^{-3} , and 1.686104×10^{-3} , respectively. Overall, the identified results highlighted that the MGO-based approach featured a fast processing time and steady convergence while retaining a high level of accuracy in the achieved solution.

Keywords: metaheuristic algorithm; parameter identification; photovoltaic cells; single-diode; double-diode; mathematical models; mountain gazelle optimization

MSC: 68T20; 90C26

1. Introduction

1.1. Motivation

The last few decades have been marked by a continuous increase in global energy needs due to demographic, industrial, and agricultural development. On the other hand, fossil fuels, causing greenhouse gas emissions and an increase in air pollution, such as coal, oil, and natural gas are experiencing dangerous exhaustion [1]. Faced with this and under the Kyoto Protocol, energy production is a critical challenge for the coming years, whether it is for developed countries to meet their needs or for developing countries to carry out their development.

In this context, several efforts have been made to discover other reliable, profitable, and renewable sources of energy [2–4]. However, due to the intrinsic volatile nature of Hybrid Renewable Energy Systems (HRESs), the evaluation of the reliability aspect of such systems to withstand unpredicted events in loaded power systems was investigated in [5]. To overcome the lack of a comparative assessment of multi-objective optimization sizing for HRESs equipped with hybrid energy storage, a comparative multi-objective framework was proposed in [6].

Among these sources are the following: solar energy coming directly from the Sun is not polluting, has no greenhouse gas emissions, is not dangerous for future generations, and is, therefore, inimitable as long as it radiates [7]. The solar Photovoltaic (PV) industry is the most-promising and powerful source of renewable energy. Photovoltaic energy comes from the direct transformation of part of the solar radiation into electrical energy. This energy conversion takes place through a PV cell exposed to light based on a physical phenomenon called the photovoltaic effect, which was discovered by the French physicist Antoine César Becquerel in 1839 [8]. Since then, several scientific pieces of research (important attempts) have led to the beginning of the actual use of PV cells to reach maturity in the last few years.

Currently, the expansion of the solar energy market is mainly due to the rising competitiveness associated with growing electricity demand, as well as the growing awareness of the potential of solar PV worldwide [9]. China is at the top of the world in terms of solar energy production. In 2022 alone, China installed 87.41 GW of new solar power (60.3% more than in 2021) to reach a cumulative capacity of 392.61 GW [10].

By the crucial importance of the use of solar energy, several aspects related to PV systems have attracted the attention of researchers and industrialists, namely the design of PV cells [11–13], maximum power point tracking [14], fault diagnosis [15,16], modeling and control [17], and the extraction of the parameters of the PV cells/panels [18]. In this paper, we are interested in extracting the main characteristic parameters of the Single-Diode Model (SDM) and the Double-Diode Model (DDM) of a solar cell. This choice of one- and two-exponential models is justified by their great importance and reputation for studying the behavior of solar cells.

1.2. Literature Review

Commonly, two famous extraction techniques are deployed: (1) the analytical [19–23] and (2) numerical ones [18,24,25]. The analytical approach is less complicated, but its accuracy is inextricably linked to the specification of some key points of the I–V curve. The accuracy of such an analytical extraction technique depends strongly on the proposed optimizer [18]. As a matter of fact, if the computed parameters are incorrectly specified, the errors can have very significant adverse effects on the PV system performance assessment [25]. Alternatively, the numerical extraction approach rests upon certain mathematical algorithms, which enables more accuracy since it allows fitting all the I–V curves. Although it is more beneficial, in terms of precision, its fitting requires more-sophisticated computation. Also, it is very important to point out that the initial values of

the parameters to be estimated should be adequately selected to avoid the non-convergence of the algorithm [26].

Currently, metaheuristic algorithms seen a substantial history to achieve the optimal solution in fine-tuning machine learning algorithms and solving continuous optimization problems [27,28]. They have gained great popularity in different application domains such as smart grid applications [29–31], Green Building Energy-Optimization Systems (GBEOSs) [32], Electric Vehicles (EVs) [33–35], the Internet of Things (IoT) [36–39], the military domain [40–42], structural health monitoring applications [43,44], Resilient Cyber-Physical Systems (RCPSs) [45,46], robotics [47,48], etc. With the growth of solar energy systems and their various design and control aspects seen as complex problems, where metaheuristics are the best candidates for addressing them, PV cell parameter identification is becoming a wide research discipline, which involves artificial intelligence and bio-inspired optimization algorithms. In this context, many new trends have been proposed to offer the possibility of enhanced task performance, high reliability, and decreased complexity and time computation over analytical, numerical, and hybrid algorithms [24,49]. In [50], the Genetic Algorithm (GA) method was the first proposed. The Particle Swarm Optimization (PSO) method was also presented in [51]. Nevertheless, the found results showed relatively high error percentages and premature convergence problems, respectively. For this, many enhanced versions of the PSO technique have been proposed like [52,53] and [54]. Alternatively, many other methods such as ABC-TRR [55], TLABC [56], and MABC [57] are intended to avoid the above problems in extracting PV cell parameters. Since the performance of all these algorithms is highly dependent on many factors like proper tuning, this makes it extremely difficult to obtain better results.

1.3. Drawbacks and Gaps in the Literature

Different optimization problems suffer from the issue of premature convergence [58,59]. To address this problem, it is mandatory that key parameter settings be well-tuned to avoid premature convergence by ensuring a balance of exploration and exploitation [60]. The best-known enhancements proposed in recently published works, especially those focusing on swarm intelligence, have been centered on the following aspects: swarm size [61], initial population [62,63], inertia weight [64], acceleration coefficients [65,66], and many others [67–69]. Although such efforts have achieved great success in dealing with low-dimensional problems [70,71], it is still a big challenge for recent approaches to address the multi-dimensionality present in the case of large-scale optimization problems.

Keeping in mind the critical trade-off between exploitation and exploration and the effect on the performance of evolutionary optimization algorithms, the achievement of the desired performance of such an algorithm relies on different levels of exploration–exploitation trade-offs at various stages of evolution. In the literature, this issue has been marked as the main drawback of the recent metaheuristics since exploration and exploitation are considered to be two complementary activities that contribute to the exploration of the search space [72]. Exploration is the process by which the search algorithm explores as much of the search space as possible, in order to escape as much as it can from converging on local optima. Exploitation, on the other hand, is the development of well-targeted approaches to find the best solutions [73]. In this way, the exploitation activity can be seen as an optimized result derived from the exploration activity, and the process of finding additional solutions continues to converge on the most-optimal ones.

To guarantee a trade-off between exploration and exploitation, various techniques have been envisaged by metaheuristic approaches, depending on their parameters and design. Indeed, the objective of avoiding premature convergence and stagnation states can be achieved by selection, replacement, or diversity operators, which ensure the diversity of solutions in the search population or memory [74]. Furthermore, the alternation of the intensification and diversification phases enables profitable exploitation of solutions considered to be the best, as well as the exploration of new search regions [75]. The alternation between the two phases is very useful, as the first guarantees improved solution

quality through local search, crossover, or hill climbing, while the second is responsible for generating new solutions due to mutation, perturbation, or restart phenomena [72].

To dynamically adjust the level of exploration and exploitation of the metaheuristic optimizer, another solution relies on the adaptation of its components or parameters according to the feedback of the search process. This solution is known as adaptive control [76].

1.4. Contribution

Improving the performance of metaheuristic algorithms remains a vital topic for complex engineering optimization problems. The ensurance of a trade-off between the exploration and exploitation is crucial to high-performance achievement. In this paper, the exploitation and exploration phases of the suggested optimizer were performed using the mountain gazelle optimizer [77], exploiting four mechanisms acting in parallel.

In summary, the main contributions of this work are as follows:

- To use the new MGO-based approach to tackle, for the first time, the problem of the PV cell/module key parameters' identification.
- To apply and experimentally validate the proposed approach to accurately approximate both the single-diode model and the double-diode model and extract their five and seven unknown parameters, respectively.
- To conduct a thorough comparison of the performance of the MGO-based approach with that of the well-established optimization algorithms of the BABCO [78], BA [78], M-SLPSO [79], GCPSO [80], TPTLBO [81], CCNMGBO [82], OBLWOA [82], FC-EPSO [83], DE [84], GWO [85], and SSA [86].
- The experimentation on two commercialized PV panels (Photowatt-PWP201, and STM6-40/36) to confirm the accuracy, stability, and convergence speed of the proposed approach.

The remainder of this paper is structured as follows. The modeling of the two different models of PV cells is presented in Section 2. The problem formulation is proposed in Section 3. The proposed MGO-based extraction method is suggested in Section 4. The executed experiments and the found results, as well as the empirical comparison with new well-known approaches are investigated in Section 5. Section 6 concludes the paper and reveals future works.

2. Different PV Cell Types' Modeling

2.1. Single Diode Model

According to the equivalent electric circuit of the SDM PV cell model [18], Kirchhoff's Current Law (KCL) can be described by Equation (1):

$$I = I_{ph} - I_{d1} - I_{sh} \quad (1)$$

where I_{ph} (A) is the photocurrent generated in the Standard Test Conditions (STCs), I_{d1} (A) is the diode D_1 current, and I_{sh} (A) is the current flowing through the shunt resistor R_{sh} (Ω). Based on Shockley diode modeling, I_{d1} is expressed by Equation (2):

$$I_{d1} = I_{sd} \left(e^{\left(\frac{V + R_s I}{\eta V_t} \right)} - 1 \right) \quad (2)$$

In Equation (2), I_{sd} (A) refers to the diode dark saturation current, R_s (Ω) is the series resistor, and V_t (V) is the junction thermal voltage at STCs.

$$V_t = \frac{k_B T_i}{q} \quad (3)$$

where η is the diode ideality factor referring to the measurement of the degree to which the diode complies with the ideal diode equation, ranging from 1–2, k_B ($1.3806503 \times 10^{-23}$ J/K),

is the Boltzmann constant, T_i (K) is the operating temperature of the PV cell, and q ($1.60217646 \times 10^{-19}$ C) is the elementary charge.

The last term of Equation (4) evaluates the current flowing through R_{sh} as described in:

$$I_{sh} = \frac{V + IR_s}{R_{sh}} \tag{4}$$

Based on the previous assumptions, Equation (1) is rewritten as follows:

$$I = I_{ph} - I_{sd} \left[e^{\left(\frac{V+IR_s}{\eta V_t} \right)} - 1 \right] - \frac{V + IR_s}{R_{sh}} \tag{5}$$

The main objective of the PV cell/module model's key parameters' identification can be achieved through optimization algorithms in order to mimic the real performance of such system. The evolved parameters are: η , R_{sh} , R_s , I_{ph} , and I_{sd} .

2.2. Double-Diode Model

To describe the double-diode model's properties, certain assumptions have to be considered in presenting a simplified version for research applications with regard to the PVSs. The equation depicting the equivalent circuit diagram of the DDM model is, thus, given by Equation (6):

$$I = I_{ph} - I_{d1} - I_{d2} - I_{sh} \tag{6}$$

Herein, the two diodes currents are given by Equation (7) and Equation (8), respectively:

$$I_{d1} = I_{sd1} \left(e^{\left(\frac{V+R_s I}{\eta_1 V_{t1}} \right)} - 1 \right) \tag{7}$$

$$I_{d2} = I_{sd2} \left(e^{\left(\frac{V+R_s I}{\eta_2 V_{t2}} \right)} - 1 \right) \tag{8}$$

Keeping in mind that V_{t1} and V_{t2} are expressed similarly as in Equation (3) and I_{sh} as in Equation (4), the PV cell output current is obtained by Equation (9):

$$I = I_{ph} - I_{sd1} \left[e^{\left(\frac{V+IR_s}{\eta_1 V_{t1}} \right)} - 1 \right] - I_{sd2} \left[e^{\left(\frac{V+IR_s}{\eta_2 V_{t2}} \right)} - 1 \right] - \frac{V + IR_s}{R_{sh}} \tag{9}$$

η_1 and η_2 are the first and second diodes' ideality factors, respectively.

Taking into account all the previous equations, the main parameters of the DDM to be identified are: I_{ph} , I_{sd1} , I_{sd2} , R_s , R_{sh} , η_1 , and η_2 . Likewise, these seven parameters will be estimated by an optimization technique with high precision and robustness.

As the module contains N_s cells, the output voltage and resistance of the module are adjusted according to specific rules:

$$\begin{cases} V' = N_s \cdot V \\ R'_s = N_s \cdot R_s \\ R'_{sh} = N_s \cdot R_{sh} \end{cases} \tag{10}$$

3. Problem Formulation

In the problem of PV module parameter estimation, the main objective is to minimize the difference between the measured and simulated current data. The difference is usually quantified by a multitude of errors such as the Root-Mean-Squared Error (RMSE), the RMSE Deviation (RMSD), the Normalized RMSD (NRMSD), the Mean Absolute Error (MAE), the MAE in Power (MAEP), the Mean Bias Error (MBE), the Mean-Squared Error (MSE), the

Sum of Squares Error (SSE), the value of the Residual Error of the Fitness Function (REFF), etc. In this paper, the objective function is expressed as follows:

$$RMSE(x) = \sqrt{\frac{1}{N} \sum_{i=1}^n (f_k(V', I, x))^2} \tag{11}$$

N represents the number of experimental data. Accordingly, (12) represents the SDM of the PV module:

$$\begin{cases} f_k(V', I, x_{sdm}) = I_{ph} - I_{sd} \left(e^{\left(\frac{V' + R'_s I}{\eta V_i} \right)} - 1 \right) - \frac{V' + R'_s I}{R'_{sh}} \\ x_{sdm} = \{ I_{ph}, I_{sd}, R'_s, R'_{sh}, \eta \} \end{cases} \tag{12}$$

In a similar form, the representation of the DDM is as follows:

$$\begin{cases} f_k(V', I, x_{ddm}) = I_{ph} - I_{sd1} \left(e^{\left(\frac{V' + R'_s I}{\eta_1 N_s V_{i1}} \right)} - 1 \right) - I_{sd2} \left(e^{\left(\frac{V' + R'_s I}{\eta_2 N_s V_{i2}} \right)} - 1 \right) - \frac{V' + R'_s I}{R'_{sh}} \\ x_{ddm} = \{ I_{ph}, I_{sd1}, I_{sd2}, R'_s, R'_{sh}, \eta_1, \eta_2 \} \end{cases} \tag{13}$$

The values of I and V' are the current and the voltage vectors measured experimentally from the PV modules. Thus, the parameters' estimation is a process that minimizes the objective function $RMSE(x)$ by adjusting the model parameters' vector x within the range of a given bound.

In this paper, the variation of the climatic conditions was taken into account according to Equations (14)–(19).

$$I_{ph,i} = \frac{G_i}{G_{STC}} (I_{ph} + \alpha_{I_{sc}} (T_i - T_{STC})) \tag{14}$$

$$E_{gap,i} = E_{gap,STC} \cdot (1 - 0.0002677 \cdot (T_i - T_{STC})) \tag{15}$$

$$I_{sd,i} = I_{sd} \cdot \left(\frac{T_i}{T_{STC}} \right)^3 \cdot e^{\left(\frac{E_{gap}}{k \cdot T_{STC}} - \frac{E_{gap}}{k \cdot T_i} \right)} \tag{16}$$

$$\eta_i = \eta \cdot \frac{T_i}{T_{STC}} \tag{17}$$

$$R_{s,i} = R_s \tag{18}$$

$$R_{sh,i} = R_{sh} \cdot \frac{G_i}{G_{STC}} \tag{19}$$

where G_i and G_{STC} are, respectively, the current irradiance and that under STCs. T_{STC} is the module temperature under STCs. $\alpha_{I_{sc}}$ is the temperature coefficient. $E_{gap,i}$ and $E_{gap,STC}$ are the gap band and that under STCs.

4. Proposed MGO-Based Extraction Method

In order to understand the general concept of the MGO, it is mandatory to bring forward its basic idea by introducing the following.

4.1. MGO's Inspiration

The mountain gazelle is a type of gazelle that lives in low densities and is distributed in large areas of the Arabian Peninsula and its surroundings, especially where Robinia

trees are grown. The mountain gazelle lives in three groups: the first includes mothers of offspring; the second includes young males; the third includes the single males' herd [87]. Although this type of animal lives in remote areas, fighting between certain components of the herd is an important feature of their coexistence. In fact, horn struggles between neighboring immature males over the environment when they reach adulthood are even more intense than those over female possession. In terms of foraging for food, the mountain gazelle's tremendous ability to run at speeds of up to 80 km per hour is a very important property that enables it to migrate distances of 120 km to graze in areas where food is abundant.

4.2. MGO Mathematical Modeling

The formulation of the MGO mathematical model is based on the simulation of the fundamental characteristics of the life of mountain gazelles and, more precisely, of their social and grouping behaviors, along with all the factors that rule the communication between their herds, reproduction, grazing, etc. [77]. One of the most-important assets of this algorithm is that the optimization processes are mainly based on more than one factor. Indeed, four factors are involved in such a dynamic process: maternity herds, solitary, bachelor male herds, territorialmales, and migration to grazing areas to search for food.

Depending on the nature of the members of the male bachelor group, who are still in the youth stage and unable to impose their dominance over the females and then carry out the reproduction process, the research population in the MGO algorithm is selected as one-third of the total population, which helps to reduce the cost compared to other options for mathematical modeling [88].

During the optimization process within the MGO, the overall best solution is identified as the adult male gazelle in the herd territory. Nevertheless, each member (Gi gazelle) can join the herd of single males, the maternity her, or solitary territorial males. On the other hand, the birth of a deer can also take place.

However, the mechanism of the MGO algorithm admits the opportunity of other solutions represented primarily by gazelles in the maternity herds. The selection is formulated so that the total population retains the stronger gazelles considered high-quality solutions and eliminates the sick and/or aged gazelles, which have a much weaker cost.

4.3. Territorial Solitary Males

Mountain gazelles live in herds that include both males, young, and females. By adulthood, the young male mountain gazelles have the strength they need to establish their dominance and continue their life cycle. At this point, newly adult males occupy a remote solitary territory. During courtship or mating season, fierce battles take place between the males, who jostle each other using their horns, as the adults try to protect their territories while the young fight for a spot in these areas, as well as for the possession of females [77]. The territory of the adult male can be established by Equation (20).

$$TSM = male_G - |(ri_1 \times BH - ri_2 \times X(t)) \times F| \times Cof_r \tag{20}$$

Herein, $male_G$ refers to the best global solution representing the position vector of the adult male. ri_1 and ri_2 are random integers, which can be taken as 1 or 2. BH is the coefficient vector of the young male herd. It can be approximated by:

$$BH = X_{ra} \times [r_1] + M_{pr} \times [r_2], ra = \left\{ \left\lceil \frac{N}{3} \right\rceil \dots N \right\} \tag{21}$$

with

$$ra = \left\{ \left\lceil \frac{N}{3} \right\rceil \dots N \right\} \tag{22}$$

X_{ra} is a random solution in the interval of ra , which represents a young male. r_1 and r_2 are values chosen randomly between 0 and 1. M_{pr} is considered as the average number of randomly selected search agents $\left\lceil \frac{N}{3} \right\rceil$, and N is the total number of herd gazelles.

In Equation (20), F is evaluated according to Equation (23).

$$F = N_1(D) \times \exp\left(2 - Iter \times \left(\frac{2}{MaxIter}\right)\right) \tag{23}$$

According to the problem dimensions, N_1 is a random number originating from the standard distribution [77]. $Iter$ and $MaxIter$ are the ongoing iterations' number and the total iterations' number, respectively.

Furthermore, in each iteration, the coefficient vector Cof_r initially randomly selected is updated in order to increase the search capability, as formulated in Equation (24).

$$Cof_i = \begin{cases} (a + 1) + r_3, \\ a \times N_2(D), \\ r_4(D), \\ N_3(D) \times N_4(D)^2 \times \cos((r_4 \times 2) \times N_3(D)) \end{cases} \tag{24}$$

The numbers $rand$, r_3 , and r_4 are randomly chosen in the interval $[0, 1]$. Also, the numbers N_2 , N_3 , and N_4 are randomly fixed according to the normal range and the problem dimensions [88]. The parameter a is expressed by:

$$a = -1 + Iter \times \left(\frac{-1}{MaxIter}\right) \tag{25}$$

4.4. Maternity Herds

As in the life cycle of all animals, maternity herds are the most-important members, which ensure the continuity of the herd's life by giving birth to new strong male gazelles. Male gazelles contribute significantly to the delivery of new gazelles and young males attempting to acquire female gazelles according to Equation (26).

$$MH = (BH + Cof_{1,r}) + (ri_3 \times male_G - ri_4 \times X_{rand}) \times Cof_{1,r} \tag{26}$$

Consider Equation (21), evaluating the young males' impact factor vector BH ; the selection of the coefficient vectors $Cof_{2,r}$ and $Cof_{3,r}$ is perform at random according to Equation (24). $male_G$ is the adult male considered as the global solution for the present repetition, while the vector position of a randomly chosen gazelle is $rand$. Otherwise, ri_3 and ri_4 are random integers of 1 or 2.

4.5. Bachelor Male Herds

Usually and according to the living conditions, the mountain deer lives for about 8 years. The breeding process begins at the age of 18 months for males and 12 months for females. The onset of winter is the typical period for the breeding season. According to zoology and sociobiology, mountain gazelles reproduce, like many mammals, by the practice of male reproduction with several females in what is known as polygamy. Most often, the female gives birth once a year, usually in April or May. While males seek to attract females and compete to mate with them, females choose selectively among available males in the herd. In this context, male dominance becomes a significant factor in the determination of mating relationships. As they mature, young male gazelles begin to gain dominance over new territories and defend them vigorously, as well as attempt to mate with females. In this critical phase, violent behavior increases between the two male groups to achieve these ends, according to Equation (27).

$$BMH = (X(t) - D) + (ri_5 \times male_G - ri_6 \times BH) \times Cof_r \tag{27}$$

Through each iteration, $X(t)$ defines the position of the gazelle vector. As defined previously, ri_5 and ri_6 are selected at random to be 1 or 2, and $male_G$ is the best solution. In addition, Cof_r is a randomly selected coefficient vector. D is established according to Equation (28) [88].

$$D = (|X(t)| + |male_G|) \times (2 \times r_6 - 1) \quad (28)$$

Here, r_6 is a number chosen randomly in the interval $[0, 1]$.

4.6. Migration to Search for Food

Mountain deer sleep most of the night and are awake most of the day, as they are active especially in the early morning and sunset. In addition to being very territorial within groups of three to eight individuals, these deer are herbivores that graze and feed on grass, leaves, or small shrubs. Usually, deer groups travel long distances to graze and search for food, taking advantage of their agile stature and their great speed in running, sprinting, and jumping. Among the important characteristics imposed by the environment in which they live, mountain deer can withstand long periods without drinking water, as they suffice with fresh herbs, dew drops, young shoots, and low-hanging tree branches, especially when their range includes the acacia tree. The mathematical formulation of the mountain gazelles' behavior is as follows (Equation (29)):

$$MSF = (ub - lb) \times r_7 + lb \quad (29)$$

Here, ub is the upper limit of the treated optimization problem, while ul is the lower limit. r_7 is a random integer ranging in the $[0, 1]$ interval.

Assuming that each generation is equal to a repetition, the production of new generations of mountain gazelles is ensured by the application of the four mechanisms described above. The addition of a new era to the total population is also considered to classify all mountain gazelles at the end of each era. Since the male adult gazelle that dominates the territory is considered the best gazelle, the classification is performed in increasing order according to the quality of the solutions. Indeed, weak or old gazelles are eliminated from the population, and only those considered to cost less and more promising are kept.

4.7. Pseudocode of the Proposed MGO Algorithm

The application of the MGO algorithm to identify the investigated PV cell/modules model parameters is summarized in Algorithm 1.

Algorithm 1: Pseudocode of the proposed MGO.

Input: The measured I–V data, the population size N , and the maximum number of iterations $MaxIter$

Output: The best solutions and the fitness value in the search space

Initialize MGO parameters;

Create a random population $X_i (i = 1, 2, \dots, N)$

Calculate the fitness levels of the gazelles

while Stopping criterion is not satisfied **do**

for each gazelle (X_i) **do**

 Load the measured I–V data

 Compute the TSM by employing Equation (20)

 Compute the MH by employing Equation (26)

 Compute the BMH according to Equation (27)

 Compute the MSF by employing Equation (29)

 Compute the fitness values of the TSM, MH, BMH, and MSF, then add them to the habitat

 Sort the entire population in ascending order

 Update the best gazelle

 Save the N best gazelles in the Max number of the population

5. Executed Experiments and Results

In this section, the MGO algorithm was used to extract the parameters of the two well-known commercial photovoltaic panels Photowatt-PWP201 and STM6-40/36. The two chosen photovoltaic panels represent the most-popular types, as monocrystalline and polycrystalline, respectively. These panels were experimented with by adopting both the SDM and DDM models. Each of these modules consists of a series of 36 connected cells. The configurations of the lower (L_b) and upper (U_b) terminals for the Photowatt-PWP201 (polycrystalline) and STM6-40/36 (monocrystalline) modules are displayed in the Table 1 [82]. The I–V experimental data used to identify the parameters of the electrical model of the Photowatt-PWP201 module were obtained under an irradiance of 1000 W/m^2 and a cell temperature of $45 \text{ }^\circ\text{C}$ [78,82]. In addition, to estimate the parameters of the electrical model of the STM6-40/36 module, real experimental data are provided for an irradiance of 1000 W/m^2 and a photovoltaic temperature of $51 \text{ }^\circ\text{C}$ [78,82].

Table 1. Parameter range of the investigated PV modules.

Parameters	Photowatt -PWP201		STP6-40/36	
	L_b	U_b	L_b	U_b
I_{ph}	0	2	0	2
I_{sd}, I_{sd1}, I_{sd2}	0	50	0	50
R_{sh}	0	2	0	0.36
R_s	0	2000	0	1000
η, η_1, η_2	1	50	1	60

The parameters of the MGO algorithm for extracting the PV model parameters (Photowatt-PWP201 and STM6-40/36) were as follows: $N = 30$ and $MaxIter = 100$. This metaheuristic MGO algorithm was compared with three other optimization methods implemented under the same conditions: Grey Wolf Optimizer (GWO), Squirrel Search Algorithm (SSA), and Differential Evolution (DE) algorithm. It is important to emphasize that all methods were tested assuming the same configuration, i.e., a number of agents of 30 and a maximum number of iterations of 100. This configuration was kept unchanged to ensure a fair comparison between the different approaches. The results obtained from the proposed approach (MGO) and the other three algorithms are presented in terms of the mean, median, minimum, maximum, and standard deviation, based on 30 runs for each algorithm. These criteria enabled us to assess the MGO’s performance in terms of accuracy, stability, and efficiency in extracting PV panel’s key parameters.

In keeping with the aim of ensuring a fair and thorough comparison of the performance of the MGO method, this comparative study also included other methods reported in the literature including the Bat–Artificial Bee Colony Optimizer (BABCO) [78], the Bat Algorithm [78], Multiswarm Spiral Leader Particle Swarm Optimization (M-SLPSO) [79], the Guaranteed Convergence Particle Swarm Optimization algorithm (GCPSO) [80], Triple-Phase Teaching–Learning-Based Optimization (TPTLBO) [81], the Criss-Cross-based Nelder–Mead simplex Gradient-Based Optimizer (CCNMGBO) [82], the quasi-Opposition-Based Learning Whale Optimization Algorithm (OBLWOA) [82], and the Fractional Chaotic Ensemble Particle Swarm Optimizer (FC-EPPO) [83]. These tests were carried out on a PC Laptop whose specifications were as follows: AMD Ryzen 7 3750H with Radeon Vega Mobile Gfx 2.30 GHz, 16 GB RAM, Windows 11, and 64 bit.

The results of identifying the parameters driving the mathematical model of the Photowatt-PWP201 polycrystalline PV module for the SDM and DDM models are tabulated in Table 2. According to these results, the MGO method performed best for the SDM, with an RMSE of 2.042717×10^{-3} , closely followed by the BABCO (2.046524×10^{-3}), M-SLPSO (2.046535×10^{-3}), and SSA (2.423290×10^{-3}) in descending order. For the DDM-based model, the best RMSE value (1.387641×10^{-3}) was also obtained by the MGO.

Based on the same investigations, the results of the parameter estimation for the STM6-40/36 monocrystalline PV module are presented in Table 3, for both the SDM and the DDM. Indeed, the results obtained with the one-diode-based model showed that the MGO method yielded the best RMSE value (1.719946×10^{-3}), followed by the BABCO (1.721921×10^{-3}), SSA (1.723619×10^{-3}), and finally, TPTLOBO (1.729800×10^{-3}). For the two-diode-based model, the best RMSE value (1.686104×10^{-3}) was achieved through the MGO approach, followed by the BABCO (1.686275×10^{-3}) and GCPSO (1.688361×10^{-3}).

As part of our comparative study of the performance of the different algorithms previously specified, each algorithm was run for 30 executions, and the descriptive statistics of the results achieved were collected for each test case about the SDM and the DDM. For each of these test cases, the following information is provided: the Mean of the best results (Mean), the Best result (Best), the Worst result (Worst), and the Standard deviation (Std.). The findings of these two tests are summarized in Tables 4 and 5. From the data presented in these two tables, it can be concluded that extremely satisfactory results were achieved by the MGO algorithm for both test cases. Overall, the MGO’s performance clearly outperformed that of the other competitive algorithms for the two investigated models.

Once the parameters of the various PV module models have been identified, it is necessary to calculate the output current corresponding to each measured voltage value. The estimated current values were compared with the measured current values to obtain the Individual Absolute Error (IAE) for each measurement. Figures 1 and 2 illustrate the results obtained by the MGO method, where the IAE is presented as a function of the measured voltage. These plots demonstrate that the IAE, when using the Photowatt-PWP201 module, did not exceed 4.00×10^{-3} for the SDM and 3.50×10^{-3} for the DDM (Figure 1a,b). For the STM6-40/36 module, it is clear that the IAE value remained below 6.00×10^{-3} with both the SDM and the DDM (Figure 2a,b).

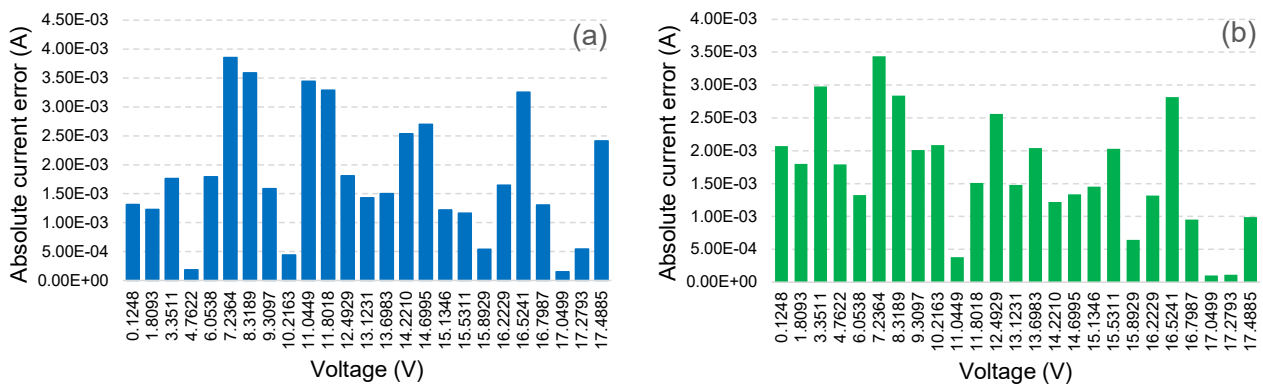


Figure 1. Current Individual Absolute Error (IAE) obtained by the MGO for the Photowatt-PWP-201 module: (a) using the SDM; (b) using the DDM.

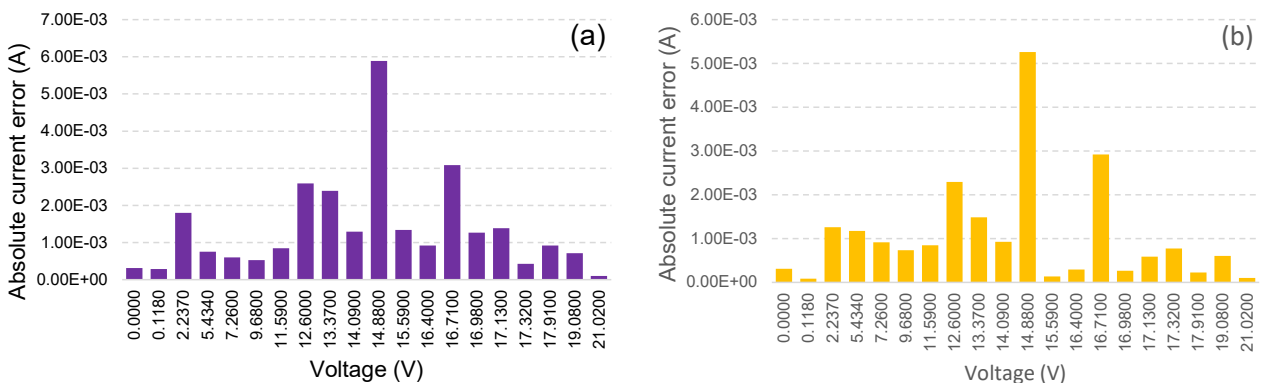


Figure 2. Current Individual Absolute Error (IAE) obtained by the MGO for the STM6-40/36 module: (a) using the SDM; (b) using the DDM.

Table 2. Comparison of the results produced by various algorithms when applied to the Photowatt-PWP201 module model.

Model	Algorithms	Parameters								RMSE $\times E^{-3}$
		I_{ph} (A)	I_{sd} (μ A)	I_{sd1} (μ A)	R_s (Ω)	R_{sh} (Ω)	η	η_1	η_2	
SDM	BABCO [78]	1.032382	2.512893	-	1.239289	744.712668	47.422839	-	-	2.046524
	BA [78]	1.044856	37.14342	-	1.318087	1495.40620	60.819912	-	-	9.771899
	M-SLPSO [79]	1.032382	2.512927	-	1.239287	744.715807	01.317305	-	-	2.046535
	TPTLBO [81]	1.030500	3.482300	-	1.201300	981.982200	48.642800	-	-	2.425100
	CCNMGBO [82]	1.030514	3.48×10^{-6}	-	1.201271	981.981900	48.642830	-	-	2.425074
	OBLWOA [82]	1.030514	3.48×10^{-6}	-	1.201271	981.984500	48.642840	-	-	2.425074
	DE	1.030515	3.443584	-	1.202534	976.587000	48.599900	-	-	2.854231
	GWO	1.028367	4.9185403	-	1.158806	1544.30824	50.000000	-	-	2.714233
	SSA	1.029777	3.529950	-	1.200619	1062.66958	48.693308	-	-	2.423290
MGO	1.030231	3.604135	-	1.198040	1033.45081	48.774295	-	-	2.042717	
DDM	BABCO [78]	1.034753	0.132561	0.312026	1.999999	591.476886	-	47.821141	42.201067	1.397480
	BA [78]	0.591915	32.63274	45.26637	0.141905	1706.06090	-	37.685352	2.455933	9.635400
	M-SLPSO [79]	1.032382	2.512910	1.00×10^{-6}	1.239288	744.713773	-	1.317304	2.499659	2.046535
	CCNMGBO [82]	1.030514	2.67×10^{-6}	3.48×10^{-6}	1.20127	981.998700	-	49.301220	48.642860	2.425000
	OBLWOA [82]	1.030514	2.17×10^{-6}	3.48×10^{-6}	1.201271	981.983200	-	49.9817404	48.642830	2.427000
	DE	1.029337	2.425199	1.1064803	1.206851	1113.0658	-	49.585175	47.312278	2.879032
	GWO	1.027243	4.787116	32.994732	1.166377	1901.8138	-	50.0000	44.840739	2.736613
	SSA	1.030626	3.311942	4.928627	1.207096	953.657	-	48.45034	36.9958	2.430466
	MGO	1.030179	3.258267	35.384629	1.1979727	1039.3818	-	48.868761	48.080506	1.387641

Table 3. Comparison of the results produced by various algorithms when applied to the STM6-40/36 module model.

Model	Algorithms	Parameters								RMSE $\times E^{-3}$
		I_{ph} (A)	I_{sd} (μ A)	I_{sd1} (μ A)	R_s (Ω)	R_{sh} (Ω)	η	η_1	η_2	
SDM	BABCO [78]	1.663903	2.048509	-	0.004267	15.93149	1.520463	-	-	1.721921
	GCPSO [80]	1.663904	1.738656	-	0.153855	573.1486	1.520302	-	-	1.729814
	TPTLOBO [81]	1.663900	1.738700	-	0.004300	15.92830	1.520300	-	-	1.729800
	DE	1.661559	5.682411	-	0.001573	785.9564	59.84265	-	-	2.891765
	GWO	1.663878	5.848076	-	0.003536	791.0496	52.56819	-	-	3.646006
	SSA	1.663668	1.908620	-	0.143125	590.8344	55.10250	-	-	1.723619
	MGO	1.663931	1.722884	-	0.154881	571.6459	54.69487	-	-	1.719946
DDM	BABCO [78]	1.663963	0.241206	6.596730	0.296972	621.1424226	-	1.363856	1.917464	1.686275
	BA [78]	1.497952	13.006836	47.796001	0.067902	929.420389	-	17.920435	3.956525	3.716638
	GCPSO [80]	1.663948	3.0995227	2.50×10^{-4}	0.295269	617.024493	-	1.636433	0.972892	1.688361
	DE	1.674689	4.774236	45.00142	0.09731012	530.006	-	59.84157	56.85469	2.819434
	GWO	1.661477	5.693952	5.023007	0.0225408	999.3609	-	60.00000	54.7395	3.591568
	SSA	1.660818	4.362375	1.246851	0.07989438	983.4837	-	59.73068	59.10384	1.759782
	MGO	1.664853	1.577101	0.390000	0.1657537	548.3743	-	57.39241	51.57719	1.686104

Table 4. RMSE statistical analysis of the Photowatt-PWP201 module for the SDM and the DDM.

Model	Algorithms	RMSE			
		Min	Max	Mean	STD
SDM	BABCO [78]	2.046524×10^{-3}	2.046424×10^{-3}	2.046524×10^{-3}	9.434855×10^{-18}
	BA [78]	9.771899×10^{-3}	1.718934×10^{-1}	3.859675×10^{-2}	4.450036×10^{-2}
	M-SLPSO [79]	2.046535×10^{-3}	2.046535×10^{-3}	2.046535×10^{-3}	3.527834×10^{-11}
	TPTLBO [81]	2.425100×10^{-3}	2.425100×10^{-3}	2.425100×10^{-3}	1.200000×10^{-17}
	DE	2.854231×10^{-3}	9.453298×10^{-3}	4.909067×10^{-3}	1.809489×10^{-3}
	GWO	2.714233×10^{-3}	2.752705×10^{-1}	4.983853×10^{-2}	9.312518×10^{-2}
	SSA	2.432902×10^{-3}	2.742507×10^{-1}	4.272723×10^{-2}	8.299818×10^{-2}
	MGO	2.042717×10^{-3}	2.0558335×10^{-3}	2.045717×10^{-3}	1.650466×10^{-3}
DDM	BABCO [78]	1.397480×10^{-3}	1.397488×10^{-3}	1.397481×10^{-3}	2.907850×10^{-9}
	BA [78]	9.635465×10^{-3}	4.404159×10^{-1}	2.362236×10^{-1}	1.850432×10^{-1}
	M-SLPSO [79]	2.046535×10^{-3}	2.051405×10^{-3}	2.046600×10^{-3}	5.093012×10^{-7}
	ED	2.879032×10^{-3}	2.463344×10^{-2}	9.559961×10^{-3}	5.874627×10^{-3}
	GWO	2.736613×10^{-3}	9.989661×10^{-2}	1.287483×10^{-2}	2.133245×10^{-2}
	SSA	2.430466×10^{-3}	2.742507×10^{-1}	7.527784×10^{-2}	1.088360×10^{-1}
	MGO	1.387641×10^{-3}	1.397421×10^{-3}	1.3902611×10^{-3}	2.992436×10^{-9}

Table 5. RMSE statistical analysis of the STM6-40/36 module for the SDM and the DDM.

Model	Algorithms	RMSE			
		Min	Max	Mean	STD
SDM	BABCO [78]	1.721921×10^{-3}	1.721921×10^{-3}	1.721921×10^{-3}	1.637363×10^{-17}
	BA [78]	4.316935×10^{-2}	3.589394×10^{-1}	2.805906×10^{-1}	1.214878×10^{-1}
	TPTLOBO [81]	1.729800×10^{-3}	1.729800×10^{-3}	1.728800×10^{-3}	4.960000×10^{-18}
	DE	2.891765×10^{-3}	4.961929×10^{-3}	3.406166×10^{-3}	3.888576×10^{-4}
	GWO	3.646006×10^{-3}	2.404023×10^{-2}	9.813445×10^{-3}	5.675926×10^{-3}
	SSA	1.743619×10^{-3}	3.107574×10^{-1}	1.367193×10^{-2}	5.612953×10^{-1}
	MGO	1.719946×10^{-3}	1.729499×10^{-3}	1.718746×10^{-3}	7.535025×10^{-17}
	DDM	BABCO [78]	1.686275×10^{-3}	1.698849×10^{-3}	1.6912799×10^{-3}
BA [78]		3.716638×10^{-2}	3.536434×10^{-1}	$1.847427E \times 10^{-1}$	1.390727×10^{-1}
FC-EP01 [83]		1.772100×10^{-3}	-	-	3.071900×10^{-10}
DE		2.819434×10^{-3}	7.931632×10^{-3}	4.289150×10^{-3}	1.061135×10^{-3}
GWO		3.591568×10^{-3}	2.317158×10^{-2}	1.179205×10^{-2}	6.004844×10^{-3}
SSA		1.759782×10^{-3}	3.107574×10^{-1}	1.836926×10^{-2}	5.674788×10^{-2}
MGO		1.686104×10^{-3}	1.781279×10^{-3}	1.69973×10^{-3}	4.873634×10^{-17}

Figures 3 and 4 show the values of the objective function obtained by the different optimization algorithms investigated during the parameter estimation process for the two PV modules (Photowatt-PWP201 and STM6-40/36) for both the mathematical SDM and DDM.

The results presented in these figures revealed that the MGO stood out for its high convergence speed right from the first iterations (around 40 iterations). Moreover, its accuracy was better than that of the other methods. These results proved that the MGO-based approach is a particularly effective alternative for solving the problems in question. This performance was due to the ability of the proposed MGO to avoid convergence to local solutions. In addition, the GWO, SSA, and DE algorithms showed a low convergence speed, particularly for the first iterations.

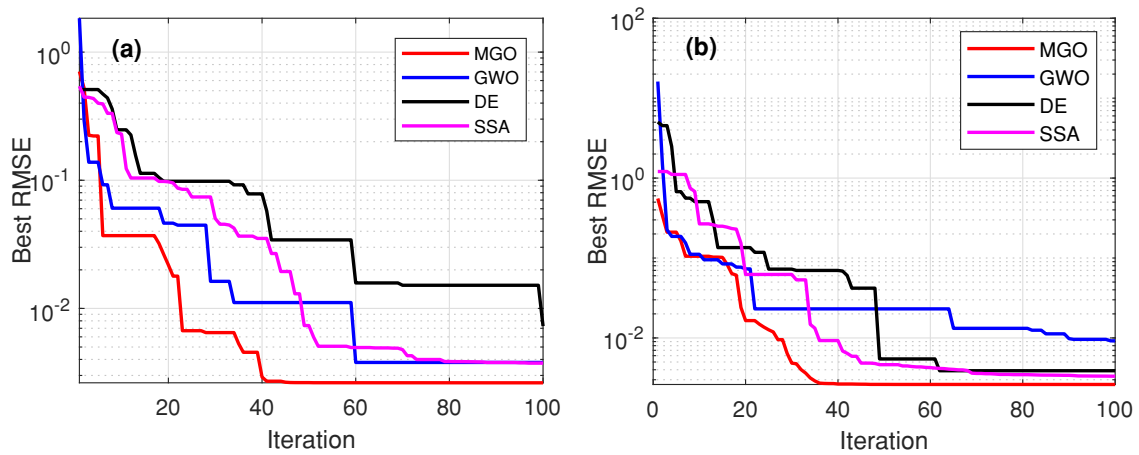


Figure 3. Comparative study of the MGO and other well-known optimization techniques in terms of the convergence characteristics for the Photowatt-PWP-201 module: (a) using the SDM; (b) using the DDM.

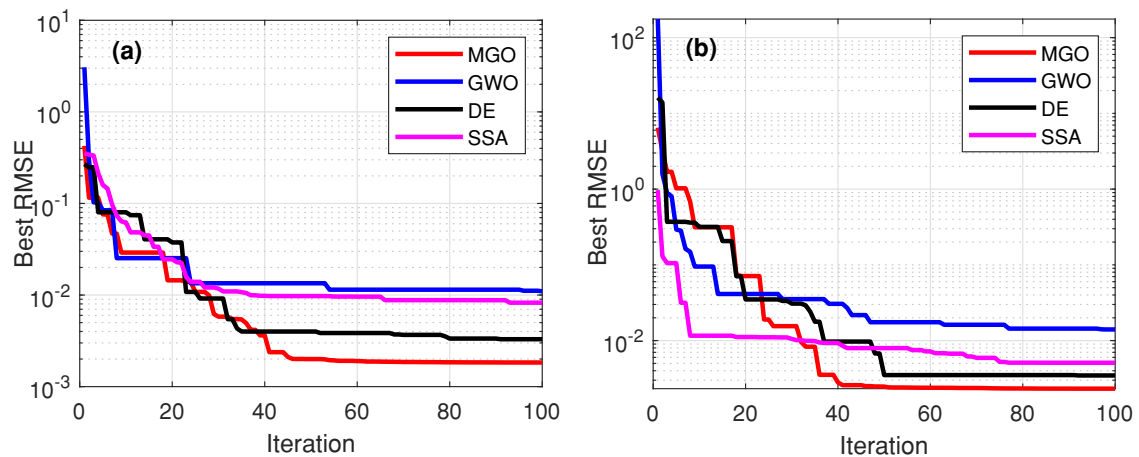


Figure 4. Comparative study of the MGO and other well-known optimization techniques in terms of the convergence characteristics for the STM6-40/36 module: (a) using the SDM; (b) using the DDM.

After obtaining the electrical parameters of the two equivalent models (SDM and DDM) of the experimented PV panels, the I–V and P–V characteristics of the two PV modules, Photowatt-PWP-201 and TM6-40/36, estimated by the proposed MGO algorithm for the SDM and the DDM are plotted.

In fact, the five key parameters of the SDM and the seven ones of the DDM PV module obtained by implementing the MGO algorithm were used to calculate the generated currents in accordance with Equations (5) and (9), respectively. As a result, the I–V and P–V characteristics were easily obtained. Accordingly, Figures 5–8 show such plots highlighting clearly that the estimated characteristics (I–V and P–V) were in good agreement with the experimental data points, thereby proving the effectiveness of the MGO compared to the other algorithms.

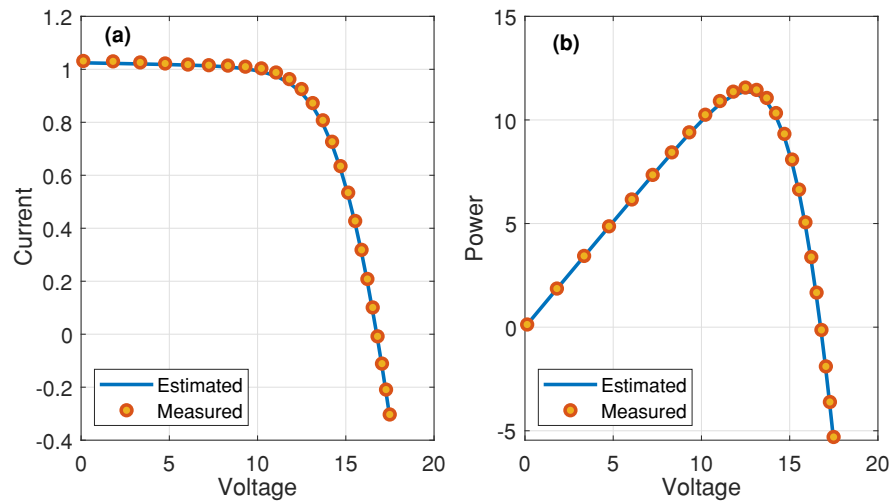


Figure 5. Comparison of measured data and simulated data obtained by the MGO of the Photowatt-PWP201 module for the SDM: (a) I-V curve. (b) P-V curve.

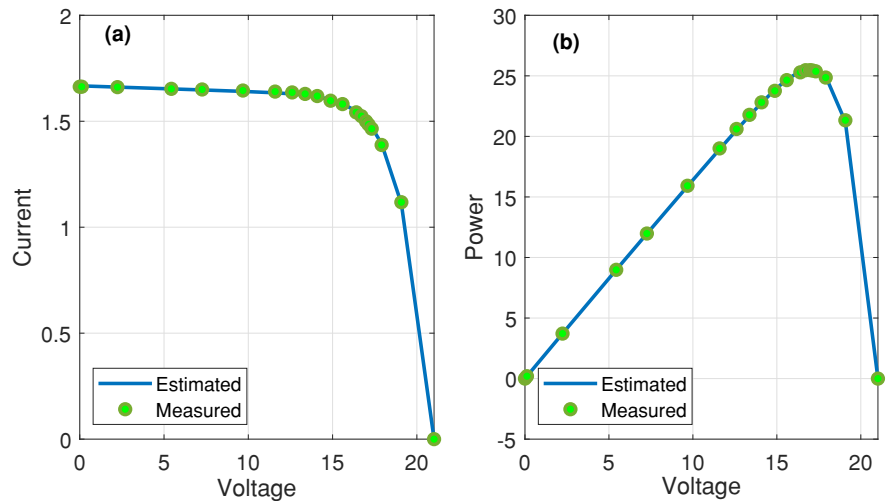


Figure 6. Comparison of measured data and simulated data obtained by the MGO of the STM6-40/36 module for the SDM: (a) I-V curve. (b) P-V curve.

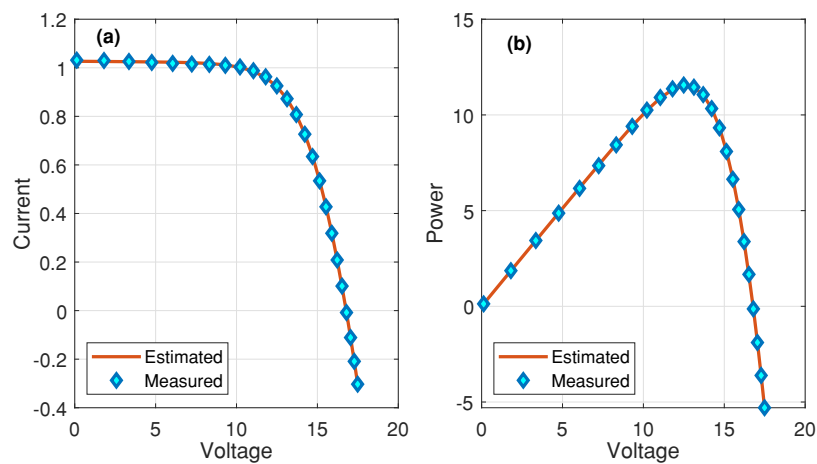


Figure 7. Comparison of measured data and simulated data obtained by the MGO of the Photowatt-PWP201 module for the DDM: (a) I-V curve. (b) P-V curve.

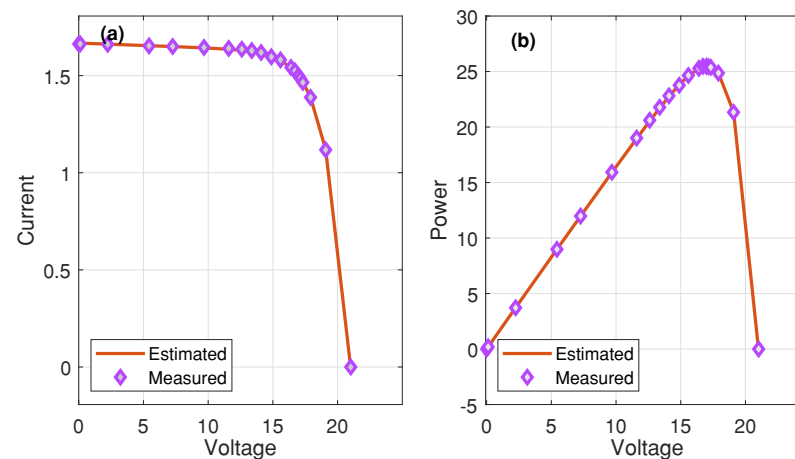


Figure 8. Comparison of measured data and simulated data obtained by the MGO of the STM6-40/36 module for the DDM: (a) I–V curve. (b) P–V curve.

6. Conclusions and Future Works

This investigation presented a new application of a Mountain Gazelle Optimizer-based approach (MGO) for identifying the key parameters of the photovoltaic Single-Diode Model (SDM) and Double-Diode Model (DDM) of technologies widely used in the literature: monocrystalline STM6-40/36 and polycrystalline Photowatt-PWP20 photovoltaic panels. The performance of the suggested MGO was assessed by many statistical indicators such as the standard deviation, Max RMSE, mean RMSE, Min RMSE, IAE, and the I–V, and P–V characteristics. The results of the experiment showed that the MGO-based method achieved superior performance and produced a competitive end result compared with other well-cited algorithms. Hence, the MGO can be a feasible alternative for parameter estimation of complex PV cell models. The experimental validation of the parameter estimation of the tested PV modules used data extracted from the I–V and P–V characteristics. For all models examined, the suggested MGO outperformed all the selected state-of-the-art optimizers by achieving the best performance in terms of accuracy, stability, and statistical data and the lowest RMSE over 30 independent runs. More concretely, the extensive experiments on the MGO showed that it outperformed the GWO algorithm by 47.17% and 46.94% on the SDM and DDM of the STM6-40/36 module, respectively. As future prospects, the MGO will be investigated to deal with many other complex optimization problems such as the maximum power point tracking issue in photovoltaic- and wind-energy-conversion systems and economic dispatch in modern power systems and smart grids.

Author Contributions: Conceptualization, R.A., S.S. and S.U.; methodology, R.A., S.S., S.U., B.N.A. and M.P.; software, R.A. and S.S.; validation, R.A., S.S. and S.U.; formal analysis, R.A., S.S. and S.U.; investigation, R.A. and S.U.; resources, S.U. and M.A.A.; data curation, R.A. and S.S.; writing—original draft preparation, R.A., S.S., S.U., B.N.A., M.A.A. and M.P.; writing—review and editing, R.A., S.S., B.N.A., M.P. and M.A.A.; visualization, R.A. and S.U.; supervision, R.A. and S.U.; funding acquisition, S.U. All authors have read and agreed to the published version of the manuscript.

Funding: This research was funded by Princess Nourah bint Abdulrahman University Researchers Supporting Project Number PNURSP2023R79, Princess Nourah bint Abdulrahman University, Riyadh, Saudi Arabia.

Institutional Review Board Statement: Not applicable.

Informed Consent Statement: Not applicable.

Data Availability Statement: Not applicable.

Acknowledgments: Princess Nourah bint Abdulrahman University Researchers Supporting Project Number PNURSP2023R79, Princess Nourah bint Abdulrahman University, Riyadh, Saudi Arabia.

Conflicts of Interest: The authors declare no conflict of interest.

Abbreviations

The following abbreviations are used in this manuscript:

PEMFC	Proton Exchange Membrane Fuel Cell
DO	Dandelion Optimizer
GWO	Grey Wolf Optimizer
GBO	Gradient-Based Optimizer
HHO	Harris Hawks Optimizer
IAEO	Improved Artificial Ecosystem Optimizer
VSDE	Vortex Search Differential Evolution
ABCDESC	Artificial Bee Colony Differential Evolution Shuffled Complex
HR	Hail Region
CO ₂	Carbon dioxide
CO	Carbon monoxide
H ₂ O	Water molecule
H ₂	Hydrogen gas
O ₂	Dioxygen gas
RE	Renewable Energy
KSA	Kingdom of Saudi Arabia
UNWTO	World Tourism Organization
COVID-19	Coronavirus Disease
EV	Electric Vehicle
ZEV	Zero-Emission Vehicle
AC	Alternating Current
GTO	Gorilla Troops Optimizer
MGTO	Modified GTO
HBO	Honey Badger Optimizer
SSE	Sum of Squared Errors
BO	Bonobo Optimizer
QOBO	Quasi-Oppositional Bonobo Optimizer
EBES	Enhanced Bald Eagle Search
DA	Dandelion Algorithm
ELM	Extreme Learning Machine
NNA	Neural Network Algorithm
ELMD	Dandelion algorithm with ELM

References

- Łukasiewicz, K.; Pietrzak, P.; Kraciuk, J.; Kacperska, E.; Cieciora, M. Sustainable Energy Development—A Systematic Literature Review. *Energies* **2022**, *15*, 8284. [[CrossRef](#)]
- Alturki, M.; Abbassi, R.; Albaker, A.; Jerbi, H. A New Hybrid Synchronization PLL Scheme for Interconnecting Renewable Energy Sources to an Abnormal Electric Grid. *Mathematics* **2022**, *10*, 1101. [[CrossRef](#)]
- Sidea, D.O.; Tudose, A.M.; Picioroaga, I.I.; Bulac, C. Two-Stage Optimal Active-Reactive Power Coordination for Microgrids with High Renewable Sources Penetration and Electrical Vehicles Based on Improved Sine–Cosine Algorithm. *Mathematics* **2023**, *11*, 45. [[CrossRef](#)]
- Zhao, L.; Jerbi, H.; Abbassi, R.; Liu, B.; Latifi, M.; Nakamura, H. Sizing renewable energy systems with energy storage systems based microgrids for cost minimization using hybrid shuffled frog-leaping and pattern search algorithm. *Sustain. Cities Soc.* **2021**, *73*, 103124. [[CrossRef](#)]
- Rasool, M.H.; Perwez, U.; Qadir, Z.; Hassan Ali, S.H. Scenario-based techno-reliability optimization of an off-grid hybrid renewable energy system: A multi-city study framework. *Sustain. Energy Technol. Assess.* **2022**, *53*, 102411. [[CrossRef](#)]
- Rasool, M.H.; Taylan, O.; Perwez, U.; Batunlu, C. Comparative assessment of multi-objective optimization of hybrid energy storage system considering grid balancing. *Renew. Energy* **2023**, *216*, 119107. [[CrossRef](#)]
- Abbassi, R.; Hammami, M.; Chebbi, S. Improvement of the integration of a grid-connected wind-photovoltaic hybrid system. In Proceedings of the International Conference on Electrical Engineering and Software Applications, Hammamet, Tunisia, 17–19 March 2013.

8. Gorjian, S.; Shukla, A. (Eds.) *Photovoltaic Solar Energy Conversion: Technologies, Applications and Environmental Impacts*; Elsevier Science: Amsterdam, The Netherlands, 2020; Volume 15, p. 8284.
9. Sara, O.P.; Paulo, R.S.; Francisco T.P. Assessment of the potential of combining wave and solar energy resources to power supply worldwide offshore oil and gas platforms. *Energy Convers. Manag.* **2020**, *223*, 113299.
10. Available online: <https://www.pv-magazine.com/2023/01/18/china-added-87-41-gw-of-solar-in-2022> (accessed on 3 April 2023).
11. Okai, V.; Chahul, H.F.; Shikler, R. Enhancement of Power Conversion Efficiency of Non-Fullerene Organic Solar Cells Using Green Synthesized Au–Ag Nanoparticles. *Polymers* **2023**, *15*, 1482. [\[CrossRef\]](#)
12. Ye, X.; Tao, Z.; Huifeng, Y.; Jingwen, W.; Pengqing, B.; Jianhui, H. Design of ultranarrow-bandgap acceptors for efficient organic photovoltaic cells and highly sensitive organic photodetectors. *J. Energy Chem.* **2022**, *72*, 388–394.
13. Zheng, Z.; Shao, Y.; Ding, C.; Li, M.; Lu, W. Rational design of ZL003-based organic dyes for highly efficient dye-sensitized solar cells: Influence of alkynyl group and π -spacers on photovoltaic performance. *J. Mol. Struct.* **2022**, *1269*, 133728. [\[CrossRef\]](#)
14. Shaolei, G.; Rabeh, A.; Houssein, J.; Alireza, R.; Kengo, S. Efficient maximum power point tracking for a photovoltaic using hybrid shuffled frog-leaping and pattern search algorithm under changing environmental conditions. *J. Clean. Prod.* **2021**, *297*, 126573.
15. Boubaker, S.; Kamel, S.; Ghazouani, N.; Mellit, A. Assessment of Machine and Deep Learning Approaches for Fault Diagnosis in Photovoltaic Systems Using Infrared Thermography. *Remote Sens.* **2023**, *15*, 1686. [\[CrossRef\]](#)
16. Liu, Y.; Ding, K.; Zhang, J.; Lin, Y.; Yang, Z.; Chen, X.; Li, Y.; Chen, X. Intelligent fault diagnosis of photovoltaic array based on variable predictive models and I–V curves. *Sol. Energy* **2022**, *237*, 340–351. [\[CrossRef\]](#)
17. Syed, H.J.; Puviarasi, R.; Chilambarasan, M.; Sarita, S.S.; Raviteja, S.; Vipin, S.; Madhavarao, S.; Sudhakar, M.; Mohanavel, V. An approach to the utilization of grid integration to analyze the performance and quality of solar photovoltaic model. *Energy Rep.* **2022**, *8*, 1029–1044.
18. Rabeh, A.; Abdelkader, A.; Mohamed, J.; Souad, C. Identification of unknown parameters of solar cell models: A comprehensive overview of available approaches. *Renew. Sustain. Energy Rev.* **2018**, *90*, 453–474.
19. Elkholly, A.; Abou El-Ela, A.A. Optimal parameters estimation and modelling of photovoltaic modules using analytical method. *Heliyon* **2019**, *5*, e02137. [\[CrossRef\]](#)
20. Martin, C.; Shady, H.E.; Ahmed, F.Z. On the root mean square error (RMSE) calculation for parameter estimation of photovoltaic models: A novel exact analytical solution based on Lambert W function. *Energy Convers. Manag.* **2020**, *210*, 112716.
21. Firoz, K.; Amir, A.A.; Fahad, A.A. Critical analysis of the limitations and validity of the assumptions with the analytical methods commonly used to determine the photovoltaic cell parameters. *Renew. Sustain. Energy Rev.* **2021**, *140*, 110753.
22. Ma, J.; Hong, D.; Wang, K.; Bi, Z.; Zhu, X.; Zhang, J. Analytical modeling and parameter estimation of photovoltaic strings under partial shading conditions. *Sol. Energy Mater. Sol. Cells* **2022**, *235*, 111494. [\[CrossRef\]](#)
23. Dris, B.H.; Mustapha, E.; El Hanafi, A.; Driss, S.; Souad, L.; Jamal, C.; Ahmed, I.; Rabya, A.; Daoudi, E.; Sergey, O. A novel hybrid numerical with analytical approach for parameter extraction of photovoltaic modules. *Energy Convers. Manag. X* **2022**, *14*, 100219.
24. Rabeh, A.; Boudjemline, A.; Abdelkader, A.; Torchani, A.; Gasmı, H.; Guesmi, T. A Numerical-Analytical Hybrid Approach for the Identification of SDM Solar Cell Unknown Parameters. *Eng. Technol. Appl. Sci. Res.* **2018**, *8*, 2907–2913.
25. Kawtar, T.; Noureddine, M.; Askar, S.S.; Mohamed, A. Numerical procedure for accurate simulation of photovoltaic modules performance based on the identification of the single-diode model parameters. *Energy Rep.* **2023**, *9*, 5532–5544.
26. Chen, X.; Ding, K.; Yang, H.; Chen, X.; Zhang, J.; Jiang, M.; Gao, R.; Liu, Z. Research on real-time identification method of model parameters for the photovoltaic array. *Appl. Energy* **2023**, *342*, 121157. [\[CrossRef\]](#)
27. Abbassi, R.; Saidi, S.; Abbassi, A.; Jerbi, H.; Kchaou, M.; Alhasnawi, B.N. Accurate Key Parameters Estimation of PEMFCs' Models Based on Dandelion Optimization Algorithm. *Mathematics* **2023**, *11*, 1298. [\[CrossRef\]](#)
28. Abdelfattah, E.; Mustapha, E.; El Hanafi, A.; Dris, B.H.; Souad, L.; Driss, S.; Imade, C.; Ismail, A. Dandelion Optimizer algorithm-based method for accurate photovoltaic model parameter identification. *Energy Convers. Manag. X* **2023**, *19*, 100405.
29. Papadimitrakı, M.; Giamarelos, N.; Stogiannos, M.; Zois, E.N.; Livanos, N.A.-I.; Alexandridis A. Metaheuristic search in smart grid: A review with emphasis on planning, scheduling and power flow optimization applications. *Renew. Sustain. Energy Rev.* **2023**, *145*, 111072. [\[CrossRef\]](#)
30. Koteswara, R.D.; Seshu, K.R.; Phani, R.L.; Singh, A.R. Enhancement of loadability and voltage stability in grid-connected microgrid network. *J. Clean. Prod.* **2023**, *374*, 133881.
31. Wu, Q.; Xue, F.; Lu, S.; Jiang, L.; Huang, T.; Wang, X.; Sang, Y. Integrated network partitioning and DERs allocation for planning of Virtual Microgrids. *Electr. Power Syst. Res.* **2023**, *216*, 109024. [\[CrossRef\]](#)
32. Qiong, W.; Gang, C.; Mohammad, K.; Banar, F.I.; Shima, R. Multi-objective optimization of IoT-based green building energy system using binary metaheuristic algorithms. *J. Build. Eng.* **2023**, *68*, 106031.
33. Leite, G.M.C.; Marcelino, C.G.; Pedreira, C.E.; Jiménez-Fernández, S.; Salcedo-Sanz, S. Evaluating the risk of uncertainty in smart grids with electric vehicles using an evolutionary swarm-intelligent algorithm. *J. Clean. Prod.* **2023**, *401*, 136775. [\[CrossRef\]](#)
34. Hubert, M.S.; Dirk, U.S. Metaheuristic for the integrated electric vehicle and crew scheduling problem. *Appl. Energy* **2023**, *339*, 120915.
35. Mohd, B.; Fareed, A.; Rizwan, M. Techno-economic assessment of grid and renewable powered electric vehicle charging stations in India using a modified metaheuristic technique. *Energy Convers. Manag.* **2023**, *284*, 116995.
36. Mohamed, A.K.; Sihem, S.; Okba, K.; Abdelhak, M.; Seyedali, M. Deep learning and metaheuristics application in internet of things: A literature review. *Microprocess. Microsyst.* **2023**, *98*, 104792.

37. Ali, S.; Tania, T.; Ali, G. Towards developing a machine learning-metaheuristic-enhanced energy-sensitive routing framework for the internet of things. *Microprocess. Microsyst.* **2023**, *96*, 104747.
38. Agostino, F. Metaheuristic algorithm for anomaly detection in Internet of Things leveraging on a neural-driven multiagent system. *Knowl.-Based Syst.* **2021**, *228*, 107241.
39. Banghua, W.; Xuebin, L.; Wameed, D.S.; Ebrahim, G.D. Optimal deploying IoT services on the fog computing: A metaheuristic-based multi-objective approach. *J. King Saud Univ.-Comput. Inf. Sci.* **2022**, *34 Pt B*, 10010–10027.
40. Ayyarao, T.S.L.V.; Ramakrishna, N.S.S.; Elavarasan, R.M.; Polumahanthi, N.; Rambabu, M.; Saini, G.; Khan, B.; Alatas, B. War Strategy Optimization Algorithm: A New Effective Metaheuristic Algorithm for Global Optimization. *IEEE Access* **2022**, *10*, 25073–25105. [[CrossRef](#)]
41. Lin, C.J.; Prasetyo, Y.T. A metaheuristic-based approach to optimizing color design for military camouflage using particle swarm optimization. *Color Res. Appl.* **2019**, *44*, 740–748. [[CrossRef](#)]
42. Ismail, M.A.; Hasan, H.T.; Sondoss, E. A military fleet mix problem for high-valued defense assets: A simulation-based optimization approach. *Expert Syst. Appl.* **2023**, *213*, 118964.
43. Naman S.B.; Abhishek, D.P.; Jegadeeshwaran, R.; Sujit, S.P.; Kaushal, A.K.; Rohan, S.G. Application of metaheuristic optimization based support vector machine for milling cutter health monitoring. *Intell. Syst. Appl.* **2023**, *18*, 200196.
44. Mohamed, O.M.; Zineb, Z.; Abdellah, N.; Seifeddine, C.; Nouzha, L.; Mohamed, E. Optimal sensor placement methodology of triaxial accelerometers using combined metaheuristic algorithms for structural health monitoring applications. *Structures* **2023**, *51*, 1959–1971.
45. Malik, M.I.; Ibrahim, A.; Hannay, P.; Sikos, L.F. Developing Resilient Cyber-Physical Systems: A Review of State-of-the-Art Malware Detection Approaches, Gaps, and Future Directions. *Computers* **2023**, *12*, 79. [[CrossRef](#)]
46. Hadeel, A.; Mohammed, A.; Jaber, S.A.; Fahd, N.A.; Anwer, M.H.; Abu Sarwar, Z.; Azza, E.O.; Amani, A.A. Chaotic marine predators optimization based task scheduling scheme for resource limited cyber-physical systems. *Comput. Electr. Eng.* **2023**, *106*, 108597.
47. Xu, Y.; Li, Q.; Xu, X.; Yang, J.; Chen, Y. Research Progress of Nature-Inspired Metaheuristic Algorithms in Mobile Robot Path Planning. *Electronics* **2023**, *12*, 3263. [[CrossRef](#)]
48. Soyeon, P.; Jongwoo, K.; Jieun, P.; Jessica, B.K.; Gunwoo, N. Design of patterns in tubular robots using DNN-metaheuristics optimization. *Int. J. Mech. Sci.* **2023**, *251*, 108352.
49. Kumar, M.; Kumar, A. An efficient parameters extraction technique of photovoltaic models for performance assessment. *Sol. Energy* **2017**, *158*, 192–206. [[CrossRef](#)]
50. Dizqah, A.M.; Maheri, A.; Busawon, K. An accurate method for the pv model identification based on a genetic algorithm and the interior-point method. *Renew. Energy* **2014**, *72*, 212–222. [[CrossRef](#)]
51. Khanna, V.; Das, B.K.; Bisht, D.; Vandana; Singh, P.K. A three diode model for industrial solar cells and estimation of solar cell parameters using pso algorithm. *Renew. Energy* **2015**, *78*, 105–113. [[CrossRef](#)]
52. Jordehi, A.R. Time varying acceleration coefficients particle swarm optimisation (tvacpso): A new optimisation algorithm for estimating parameters of pv cells and modules. *Energy Convers. Manag.* **2016**, *129*, 262–274. [[CrossRef](#)]
53. Nunes, H.G.G.; Pombo, J.A.N.; Mariano, S.J.P.S.; Calado, M.R.A.; Felipe de Souza, J.A.M. A new high performance method for determining the parameters of pv cells and modules based on guaranteed convergence particle swarm optimization. *Appl. Energy* **2018**, *211*, 774–791. [[CrossRef](#)]
54. Jordehi, A.R. Enhanced leader particle swarm optimisation (elpso): An efficient algorithm for parameter estimation of photovoltaic (pv) cells and modules. *Sol. Energy* **2018**, *159*, 78–87. [[CrossRef](#)]
55. Wu, L.; Chen, Z.; Long, C.; Cheng, S.; Lin, P.; Chen, Y.; Chen, H. Parameter extraction of photovoltaic models from measured I-V characteristics curves using a hybrid trust region reflective algorithm. *Appl. Energy* **2018**, *232*, 36–53. [[CrossRef](#)]
56. Chen, X.; Xu, B.; Mei, C.; Ding, Y.; Li, K. Teaching-learning-based artificial bee colony for solar photovoltaic parameter estimation. *Appl. Energy* **2018**, *212*, 1578–1588. [[CrossRef](#)]
57. Jamadi, B.M.; Merrikh-Bayat, F. Very accurate parameter estimation of single- and double-diode solar cell models using a modified artificial bee colony algorithm. *Int. J. Energy Environ. Eng.* **2016**, *7*, 13–25. [[CrossRef](#)]
58. Li, D.; Guo, W.; Lerch, A.; Li, Y.; Wang, L.; Wu, Q. An Adaptive Particle Swarm Optimizer with Decoupled Exploration and Exploitation for Large Scale Optimization. *Swarm Evol. Comput.* **2021**, *60*, 100789. [[CrossRef](#)]
59. Premkumar, M.; Shankar, N.; Sowmya, R.; Jangir, P.; Kumar, C.; Abualigah, L.; Derebew, B. A reliable optimization framework for parameter identification of single-diode solar photovoltaic model using weighted velocity-guided grey wolf optimization algorithm and Lambert-W function. *IET Renew. Power Gener.* **2023**, *17*, 2711–2732. [[CrossRef](#)]
60. Irudayaraj, A.X.R.; Wahab, N.I.A.; Veerasamy, V.; Premkumar, M.; Radzi, M.A.M.; Sulaiman, N.B.; Haes Alhelou, H. Decentralized frequency control of restructured energy system using hybrid intelligent algorithm and non-linear fractional order proportional integral derivative controller. *IET Renew. Power Gener.* **2023**, *17*, 2009–2037. [[CrossRef](#)]
61. Premkumar, M.; Sowmya, R.; Ramakrishnan, C.; Pradeep, J.; Essam, H.H.; Sanchari, D.; Nallapaneni, M.K. An efficient and reliable scheduling algorithm for unit commitment scheme in microgrid systems using enhanced mixed integer particle swarm optimizer considering uncertainties. *Energy Rep.* **2023**, *9*, 1029–1053. [[CrossRef](#)]
62. Chen, W.-C.; Tai, Y.-C.; Wang, M.-W.; Tsai, H.-C. Parameter optimization of etching process for a LGP stamper. *Neural Comput. Appl.* **2013**, *23*, 1539–1550. [[CrossRef](#)]

63. Chen, W.-C.; Kurniawan, D. Process parameters optimization for multiple quality characteristics in plastic injection molding using Taguchi method, BPNN, GA, and hybrid PSO-GA. *Int. J. Precis. Eng. Manuf.* **2014**, *15*, 1583–1593. [CrossRef]
64. Li, M.; Chen, H.; Shi, X.; Liu, S.; Zhang, M.; Lu, S. A multi-information fusion ripple variables with iteration inertia weight PSO algorithm and its application. *Appl. Soft Comput.* **2019**, *84*, 105677. [CrossRef]
65. Ji, K.; Zhao, P.; Zhou, X.; Chen, Y.; Dong, Z.; Zheng, J.; Fu, J.; Zhou, H. Uniform Initialization in Response Space for PSO and its Applications. *Appl. Math. Comput.* **2022**, *431*, 127351. [CrossRef]
66. Rezaee, A.J.; Jasni, J. Parameter selection in particle swarm optimisation: A survey. *J. Exp. Theor. Artif. Intell.* **2013**, *25*, 527–542. [CrossRef]
67. Chen, Y.; Li, L.; Xiao, J.; Yang, Y.; Liang, J.; Li, T. Particle swarm optimizer with crossover operation. *Eng. Appl. Artif. Intell.* **2018**, *70*, 159–169. [CrossRef]
68. Liu, W.; Wang, Z.; Liu, X.; Zeng, N.; Bell, D. A novel particle swarm optimization approach for patient clustering from emergency departments. *IEEE Trans. Evol. Comput.* **2013**, *23*, 718–724. [CrossRef]
69. Li, J.; Zhang, J.Q.; Jiang, C.J.; Zhou, M.C. Composite particle swarm optimizer with historical memory for function optimization. *IEEE Trans. Cybern.* **2017**, *45*, 2350–2363. [CrossRef]
70. Sibalija, T.V. Particle swarm optimisation in designing parameters of manufacturing processes: A review. *Appl. Soft Comput.* **2019**, *84*, 105743. [CrossRef]
71. Sengupta, S.; Basak, S.; Peters, R.A. Particle swarm optimization: A survey of historical and recent developments with hybridization perspectives. *J. Mach. Learn. Knowl. Extract.* **2019**, *1*, 157–191. [CrossRef]
72. Anthony, T.; Anthony, S.M.; Ashok, K. Exploration in neo-Hebbian reinforcement learning: Computational approaches to the exploration–exploitation balance with bio-inspired neural networks. *Neural Netw.* **2022**, *151*, 16–33.
73. Nikhil, A.; Siba, S.M. Switching from exploration to exploitation in gravitational search algorithm based on diversity with Chaos. *Inf. Sci.* **2023**, *635*, 298–327.
74. Wang, P.; Xue, B.; Liang, J.; Zhang, M. Feature Selection Using Diversity-Based Multi-objective Binary Differential Evolution. *Inf. Sci.* **2023**, *626*, 586–606. [CrossRef]
75. Atefeh, R.K.; Fatemeh, G.J.; Iman, S.; Mostafa, H.K. Utilizing hybrid metaheuristic approach to design an agricultural closed-loop supply chain network. *Expert Syst. Appl.* **2023**, *217*, 119504.
76. Souhail, D.; Alaeddine, Z. Adaptive iterated stochastic metaheuristic to optimize holes drilling path in manufacturing industry: The Adaptive-Dhouib-Matrix-3 (A-DM3). *Eng. Appl. Artif. Intell.* **2023**, *120*, 105898.
77. Benyamin, A.; Farhad, S.G.; Nima, K.; Seyedali, M. Mountain Gazelle Optimizer: A new Nature-inspired Metaheuristic Algorithm for Global Optimization Problems. *Adv. Eng. Softw.* **2022**, *174*, 103282.
78. Aoufi, B.; Hachana, O.; Sid, M.A.; Giuseppe, M.T. Precise and fast parameter identification of monocrystalline, polycrystalline, and mono-facial photovoltaic modules using a new Bat Artificial Bee Colony optimizer. *J. Comput. Electron.* **2022**, *21*, 491–512. [CrossRef]
79. Nunes, H.G.G.; Silva, P.N.C.; Pombo, J.A.N.; Mariano, S.J.P.S.; Calado, M.R.A. Multiswarm spiral leader particle swarm optimisation algorithm for PV parameter identification. *Energy Convers. Manag.* **2020**, *225*, 113388. [CrossRef]
80. Nunes, H.G.G.; Pombo, J.A.N.; Mariano, S.J.P.S.; Calado, M.R.A. Suitable mathematical model for the electrical characterization of different photovoltaic technologies: Experimental validation. *Energy Convers. Manag.* **2021**, *231*, 113820. [CrossRef]
81. Liao, Z.; Chen, Z.; Li, S. Parameters Extraction of Photovoltaic Models Using Triple-Phase Teaching-Learning-Based Optimization. *IEEE Access* **2020**, *8*, 69937–69952. [CrossRef]
82. Wang, D.; Sun, X.; Kang, H.; Shen, Y.; Chen, Q. Heterogeneous differential evolution algorithm for parameter estimation of solar photovoltaic models. *Energy Rep.* **2022**, *8*, 15249–15285. [CrossRef]
83. Yousri, D.; Thanikanti, S.B.; Allam, D.; Ramachandramurthy, V.K.; Eteiba, M.B. Fractional chaotic ensemble particle swarm optimizer for identifying the single, double, and three diode photovoltaic models' parameters. *Energy* **2020**, *195*, 116979. [CrossRef]
84. Manoharan, P.; Chandrasekaran, K.; Thankkapan, D.; Somasundaram; David, T.S.J.; Pradeep, J.; Hassan, H.A. A reliable optimization framework using ensembled successive history adaptive differential evolutionary algorithm for optimal power flow problems. *IET Gener. Transm. Distrib.* **2023**, *17*, 1333–1357.
85. Mirjalili, S.; Mirjalili, S.M.; Lewis, A. grey wolf optimizer. *Adv. Eng. Softw.* **2014**, *69*, 46–61. [CrossRef]
86. Mohit, J.; Vijander, S.; Asha, R. A novel nature-inspired algorithm for optimization: Squirrel search algorithm. *Swarm Evol. Comput.* **2019**, *44*, 148–175.
87. Palestine Mountain Gazelle Officially an Endangered Species. Available online: <https://www.newarab.com/news/palestine-mountain-gazelle-officially-endangered-species> (accessed on 16 June 2023).
88. Chandrasekaran, K.; Thaveedhu, A.S.R.; Manoharan, P.; Vijayarajan, P. Optimal estimation of parameters of the three-diode commercial solar photovoltaic model using an improved Berndt-Hall-Hall-Hausman method hybridized with an augmented mountain gazelle optimizer. *Environ. Sci. Pollut. Res.* **2023**, *30*, 57683–57706. [CrossRef]

Disclaimer/Publisher's Note: The statements, opinions and data contained in all publications are solely those of the individual author(s) and contributor(s) and not of MDPI and/or the editor(s). MDPI and/or the editor(s) disclaim responsibility for any injury to people or property resulting from any ideas, methods, instructions or products referred to in the content.